Mem. S.A.It. Vol. 86, 123

Memorie della

The GeV flare in PSR B1259-63 during the 2010/2011 periastron passage

B. van Soelen and P.J. Meintjes

Department of Physics, University of the Free State, Bloemfontein, 9300, South Africa
e-mail: vansoelenb@ufs.ac.za

Abstract. The gamma-ray binary star system PSR B1259-63 is unique among the five known systems since it is the only one where a radio pulsar has been directly detected. Approximately 30 days after the 2010 periastron passage *Fermi*-LAT detected a rapid increase, at a time when emission at other wavelengths was already decreasing. Here we discuss the possible influence of second-order Fermi acceleration if sufficiently strong turbulence develops in the shock. Following the steady-state approximation as presented by Stawarz & Petrosian (2008) we calculate the expected shape of the light curve produced under this processes, if it is assumed that in the final emission region the particles are subject to mild Doppler boosting ($\Gamma = 2$). In this first approximation, the modelled light curve shows a rapid rise beginning $\sim$ 28 days after periastron, and peaks $\sim$ 42 days after.

Key words. Gamma-ray binaries - individual: PSR B1259-63

1. Introduction

The gamma-ray binary star system PSR B1259-63 which consists of a 48 ms pulsar in a 3.4 year orbit ($e \approx 0.8$) around a Be star ($M_\star \approx 31 M_\odot$) (Negueruela et al. 2011), is unique among the five known gamma-ray binaries because it is the only one where a radio pulsar has been directly detected in the system (Johnston et al. 1992). Close to periastron, the pulsar appears to pass close to or behind the Be star's circumstellar disc and is eclipsed. It is, however, during this period that an increase in non-thermal/unpulsed emission is detected from radio to TeV gamma-ray. The non-thermal emission in radio, X-ray and TeV gamma-rays has been fairly consistent during the previous periastron passages (Johnston et al. 2005; Moldón et al. 2011; Chernyakova et al. 2009; Pavlov et al. 2011; Abramowski et al. 2013)

Before the observations undertaken with *Fermi* during 2010/2011, it was unclear whether PSR B1259-63 would be a GeV source. Various modelling suggested that the system would, at most, be only slightly detectable with *Fermi*. This made the subsequent bright detection highly unexpected.

Near to the previous periastron (2010/2011) observations with *Fermi* only detected PSR B1259-63 by integrating from $\tau = -20$ to $\tau = 0$ d (where τ is the time from periastron; Abdo et al. 2011). This resulted in a faint detection, which lasted until $\tau =\sim +18$ d. The resulting flux during this period was $F = (0.9 \pm 0.3_{\rm stat} \pm 0.4_{\rm sys}) \times 10^{-10}$ erg cm^{-2} s^{-1} with a photon index of $\Gamma = 2.4 \pm 0.2_{\rm stat} \pm 0.5_{\rm sys}$. There was a subsequent rapid increase

in flux (above 100 MeV) from about $\tau = +30$ d with an average flux of $F = (4.4 \pm 0.3_{\rm stat} \pm 0.76_{\rm sys}) \times 10^{-10}$ erg cm^{-2} s^{-1}, a photon index of $\Gamma = 1.4 \pm 0.6_{\rm stat} \pm 0.2_{\rm sys}$ and a cut-off at $E = 0.3 \pm 0.1_{\rm stat} \pm 0.1_{\rm sys}$ GeV (Abdo et al. 2011). The resulting peak luminosity was $L_\gamma \approx 8 \times 10^{35}$ erg s^{-1} for an assumed distance of $d = 2.3$ kpc. This is ~ 100 per cent of the spin-down luminosity of the pulsar ($P = 47.75$ ms, $\dot{P} = 2.28 \times 10^{-15}$, Shannon, Johnston & Manchester 2014). Around the 2014 periastron passage, there has been a repeated observation of gamma-ray activity from PSR B1259-63, confirming the binary nature of these observations (e.g. Wood et al. 2014). The shape of the gamma-ray spectrum, a power-law with exponential cut-off, is similar to that seen in gamma-ray pulsars (see e.g. Abdo et al. 2013; Dubus 2013) though there is no detected pulsed signal from the system.

A number of different models were put forward to explain the GeV emission: Khangulyan et al (2012) proposed that the emission was inverse Compton scattering from the cold pulsar wind; Kong et al. (2012) proposed that it was Doppler boosted synchrotron emission originating in the outer shock front; while most recently Dubus & Cerutti (2013) considered inverse Compton scattering of X-ray photons.

Below we discuss a different possibility, that the GeV gamma-ray emission is the result of turbulence induced particle acceleration in the shock-front which results in a Maxwellian-like particle distribution and subsequent inverse Compton scattering.

2. Particle acceleration

Stawarz & Petrosian (2008) investigated the effects of second-order Fermi particle acceleration in a turbulent plasma, under the influence of particle cooling. These authors found that the combined effect of second-order particle acceleration and radiative cooling resulted in a steady state solution with a Maxwellian-like particle distribution with the approximate form

$$n_e(\gamma) = n_0 \gamma^2 \exp\left[-\frac{1}{a}\left(\frac{\gamma}{\gamma_{\rm equ}}\right)^a\right], \quad (1)$$

where n_0 is the normalization, $\gamma_{\rm equ}$ is the equilibrium Lorentz factor of the particle determined by the acceleration and cooling time-scales, and the parameter a depends on the radiative cooling and turbulent spectrum. For synchrotron and Thomson limit inverse Compton scattering, $a = 3-q$, while for Klein-Nishina inverse Compton scattering $a = 1.5-q$ (and $q < 1.5$). Here, q is the turbulence spectral index, i.e. $q = 5/3$ for Kolmogorov turbulence and $q = 3/2$ for a Kreichnan turbulence spectrum. This is, of course, an approximation and the more detailed analysis (as discussed in Stawarz & Petrosian 2008) shows that the particle distribution can develop with, for example, a power-law tail. However, we will take this as a first approximation of the required particle distribution.

The problem faced with second-order Fermi acceleration is that the time scales required to accelerated the particles are often considered too long: here the acceleration timescale is (following the notation of Stawarz & Petrosian 2008)

$$t_{\rm acc} = \frac{\lambda_2}{\zeta \beta_A^2 c}\left(\frac{p_0 c}{eB\lambda_2}\right)^{2-q} \chi^{2-q} \quad (2)$$

where, λ_2 is the maximum Alfvén wavelength, $\zeta = (\delta B/B)^2$ is a measure of the change in the magnetic field strength B, $(\beta_A c)$ is the Alfvén velocity, e is the electron charge, and $\chi = p/p_0$ is the dimensionless particle momentum, in terms of the injected particle momentum, p_0. The resulting time scale is longer than obtained from, for example, first order acceleration in a shock. However, if sufficiently strong turbulence can develop, a particle may become trapped allowing enough time for the second-order acceleration to become important. If such a Maxwellian-like particle distribution does develop, inverse Compton scattering of optical photons from the Be star could produce a spectrum which is consistent with the spectrum observed by *Fermi*. Further, by introducing variations in $\gamma_{\rm equ}$ due to the changing conditions in the shock front as the pulsar orbits around the Be star, and by introducing geometric dependent events, such as Doppler boosting, it may be possible to reproduce the observed GeV light curve.

3. Development of turbulence

The interaction between the pulsar and stellar wind presents interesting possibilities for the development of turbulence. The large velocity difference between the pulsar and stellar wind could lead to Kelvin-Helmholtz instabilities forming along the shock front (e.g. Bosch-Ramon & Barkov 2011), while numerical simulations have shown their development in colliding wind binaries (Bosch-Ramon et al. 2012; Lamberts et al. 2012). This could then lead to the development of turbulent regions within which second-order Fermi acceleration could occur. The dispersive nature of Kelvin–Helmholtz instabilities results in the fact that not all modes (k-number) are equally affected by this large velocity gradient. If certain wave-modes can develop in the pulsar-stellar wind interface it will grow, resulting in mixing which will tend to smooth the large velocity gradient, allowing more modes to develop and grow.

4. Model outline

The outlined model is such, high energy particles, either from the cold pulsar wind, or re-accelerated particles from the post-shock region are trapped within regions of turbulence which develop along the shock front. This will result in these particles undergoing a process of acceleration and radiative cooling, leading to the development of a Maxwellian-like particle distribution. Subsequent inverse Compton cooling will produce the spectrum observed with *Fermi*. Given that the bright point in the GeV light curve occurs near inferior conjunction, when the shock front is directed towards us, suggests a geometric component is required to explain the light curve. We assume here that the particles are undergoing mild Doppler boosting from the bulk flow in the shock front (Bogovalov et al. 2008) resulting in a preferential flux close to inferior conjunction. In addition, the change in condition of the surrounding medium near the pulsar, around periastron, creates a variation in $\gamma_{\rm eq}$ and a subsequent shift in the peak of the observed emission.

Here, as a first approximation, we consider only the steady state solution presented by Stawarz & Petrosian (2008), assume $\Gamma = 2$ and calculate $\gamma_{\rm eq}$ from $t_{\rm acc} = t_{\rm ic}$, where we have only considered inverse Compton cooling in the Thomson regime. The inverse Compton cooling rate, $t_{\rm ic} \propto 1/(\gamma U)$, is inversely proportional to the photon energy density, U, which we have calculated from the stellar photon energy density, taking into account the reduction due to Doppler boosting. The acceleration time scale, equation (2), depends on the stellar density, through the Alfvén speed, and the maximum allowed Alfvén wavelength λ_2.

The density of the medium is determined by the density of the stellar wind and circumstellar disc at the position of the pulsar. The density of the disc is calculated by (Hummel & Vrancken 2000)

$$\rho_{\rm disc}(r_c, z) = \rho_0 \left(\frac{R_\star}{r_c}\right)^{\varpi} \exp\left(-0.5\left[\frac{z}{H(r_c)}\right]^2\right), \quad (3)$$

where r_c is the radial distance in cylindrical coordinates (where r_c lies in the plane of the disc), ρ_0 is the density at the base of the disc, ϖ determines how the density scales with radial distance and

$$H(r_c) = a\frac{R_\star}{v_{\rm crit}}\left(\frac{r_c}{R_\star}\right)^{1.5},$$

with a the speed of sound and $v_{\rm crit}$ the critical velocity. Here we have adopted $\rho_0 = 10^{-10}$ g cm^{-3}, $\varpi = 3.055$, $T_{\rm disc} = 18\,000$ K and $\mu = 1.9$ (e.g. van Soelen et al. 2012), and the disc is assumed to lie at an inclination of 50° to the plane of the orbit.

The density of the stellar wind is calculated from (e.g. Kong et al. 2011; Waters et al. 1988)

$$\rho_{\rm star}(r) = \frac{\dot{M}}{4\pi f r^2 v_{\rm w}(r)},$$

where $\dot{M}/f$ is the fraction of mass outflow in the stellar wind, and $v_{\rm w}$ is the speed of the stellar wind given by

$$v_{\rm w}(r) = v_{0,\rm polar} + (v_\infty - v_{0,\rm polar})\left(1 - \frac{R_\star}{r}\right)^{1.5}.$$

Here, r is the binary separation, and we have assumed $v_{0,\rm polar} = 10^6$ cm s^{-1} and $v_\infty =$

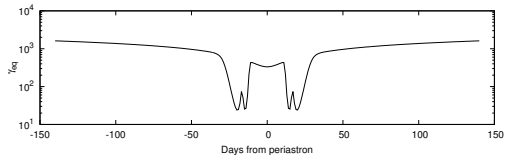

Fig. 1. Variation in γ_{eq} around periastron (as measured in the co-moving bulk frame).

10^8 cm s^{-1} (Kong et al. 2011), and $\dot{M}/f \sim 6 \times 10^{-8} M_\odot$ yr^{-1} (Negueruela et al. 2011).

The two remaining parameters ζ and λ_2 have been chosen so that a value of $\gamma_{eq} \sim 1000$ is found near periastron, which produces a reasonable match to the spectral shape observed by *Fermi*. We have taken $\zeta = 0.25$ and, given the uncertainty in the maximum allowed wavelength, allowed λ_2 to scale as some constant fraction f of the stand–off shock distance R_S, i.e. $\lambda_2 = fR_S$. The stand–off shock distance is determined by

$$R_s = \frac{\eta^{1/2}}{1+\eta^{1/2}} D,$$

where D is the binary separation, and η is ratio of the momentum flux of the pulsar and stellar wind. We adopted $\eta_{min} = 0.01$ and $\eta_{max} = 0.1$ (appropriate for the circumstellar disc and stellar wind respectively) and produce a smooth transition by scaling η in terms of the ram pressure of the stellar wind/disc (ρv^2). It is found that $f \approx 2 \times 10^{-4}$ produced a reasonable match for the gamma-ray spectrum. The variation in γ_{eq} is shown in Fig. 1

A first approximation of the light curve is calculated by determining the isotropic inverse Compton scattering rate, using the full scattering crossing section, such as given in, for example, Blumenthal & Gould (1970). The target photon number density is calculated from the photon energy density, taking into account Doppler boosting, while the electron density is determined by equation (1). The normalization of the observed flux will depend on the normalization of the emitting electron distribution. For a first approximation we require only that

$$\int_0^\infty d\gamma \left(\gamma mc^2\right) n_e(\gamma) = \text{constant}.$$

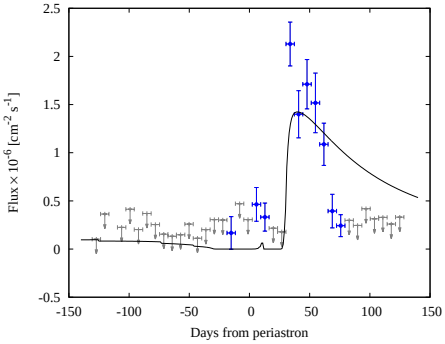

Fig. 2. Preliminary result for the modelled light curve for the gamma-ray emission, scaled to arbitrary units, compared to the flux detected by *Fermi*-LAT during around the 2010/2011 periastron passage.

It can be shown that this integral is proportional to γ_{eq}^4 and therefore we set $n_0 \propto \gamma_{eq}^{-4}$.

Assuming a cone shape for the shock outflow, we have calculated the Doppler boosting factor by calculating the minimum angle between the outflow (determined from the opening angle of the shock) and the line-of-sight to the observer. The opening angle of the shock is estimated from the opening angle of the shock contact surface (Eichler & Usov 1993; Bogovalov et al. 2008)

$$\theta = 2.1\eta^{1/3}\left(1 - \frac{\eta^{2/5}}{4}\right).$$

The resultant light curve (in arbitrary units) is compared to the *Fermi* light curve in Fig. 2.

5. Discussion & conclusion

The shape of the modelled light curve shown in Fig. 2 predicts a much slower decay in the observed flux after the flare. However, this is a first approximation and the correct modelling of the normalization of the particle spectrum, as well as the emission region is not considered. A more refined model may be able to produce a better approximation (see discussion below).

This simplified model does, however, produce a rapid rise in observed flux, shortly after periastron (starting $\tau \sim +28$ d, peaking

$\tau \sim +42$ d) and not during periastron nor near the disc crossing, which is in line with the general trend of of the GeV gamma-ray observations.

There are a number of assumptions and approximations made in this first approximation which can be extended and further investigated. Firstly reasons from the over prediction of the flux in the period following the initial flare in the GeV spectrum should be considered. Possible reasons for this include:

1. The particle distribution is only normalized to assume there it is some constant value, while the particle energy will depend on the amount of energy that enters into the turbulent region. This total energy should be limited by the spin-down luminosity of the pulsar. Following on this no assumption has been made about the size of the emission region.
2. A steady state solution is assumed to calculate the electron distribution, following Stawarz & Petrosian (2008). Since the inverse Compton cooling time at $\sim$ 30 d after periastron is

$$t_{\rm IC} \approx 0.6 \left(\frac{\gamma}{10^3}\right)^{-1} \left(\frac{r}{61.2 R_\star}\right)^2 \ {\rm d}$$

   a full time-dependent solution may be more appropriate. Given this longer cooling time, it is required that particles must become trapped within turbulent regions close to the pulsar/star binary system to provide sufficient time for particle acceleration to produce the Maxwellian-like distribution. As the binary separation increases following periastron, there will be a subsequent decrease in the target photon energy density and particle density, and an increase in the radiative (inverse Compton) cooling time. Since the combined effects of second-order acceleration and radiative cooling is required to produce the Maxwellian-like distribution (Stawarz & Petrosian 2008), less particles may be accelerated to form this spectrum. In addition we have not considered other cooling effects, and as the pulsar moves into regions of lower ambient density adiabatic cooling can become the dominant process.
3. Only one configuration for the Doppler boosting as been consider, and a different choice of Γ and direction of bulk flow relative to our line of sight will produce different results.

The combination of these effects, could explain the over prediction following the rapid rise in the emission (Fig. 2). Secondly, additional cooling process which may become dominant within the circumstellar disc have not been considered. Near the disc crossing the lower value of $\gamma_{\rm eq}$ (Fig. 1) would produce inverse Compton emission in the keV to MeV energy range. However, during this time, because of the higher density in the circumstellar disc, Coulomb and bremsstrahlung losses will become important (e.g. Neronov & Chernyakova 2007), an effect not considered here, which will alter the value of $\gamma_{\rm eq}$. In addition, a possible shorter escape time, due to a more confined shock within the disc, may not provided sufficient time to allow the second-order acceleration to become important.

Lastly the chosen orientation of the disc has implications for the observed radio pulsations which are eclipsed from $\sim$ 17 days before periastron until $\sim$ 17 days after. A higher density is required to restrict $\gamma_{\rm equ}$ such that the rapid rise in GeV emission is only observed a few 10s of days after periastron, but this is constrained by the requirement that the radio pulsar is observable. Since the higher density is confined to the circumstellar disc (equation 3), the disc may be orientated so that the line of sight through the disc is low enough that the pulsed emission is still visible.

While there are a number of aspects that are still being investigated, the model is able to produce a rapid rise in GeV flux after periastron, with a spectrum compatible with that observed with *Fermi*-LAT. This may point to an alternative explanation for the *Fermi* flare.

References

Abdo, A. A., Ackermann, M., Ajello, M. et al. 2011, ApJ, 736, L11

Abdo, A. A., Ajello, M., Allafort, A., et al. 2013. ApJS, 208, 17
Abramowski A. et al. (H.E.S.S. Collaboration), 2013, A&A, 551, A94
Blumenthal, G. R., Gould, R. J. 1970, Reviews of Modern Physics, 42, 237
Bogovalov, S.V., et al. 2008, MNRAS, 387, 63
Bosch-Ramon, V., Barkov, M.V. 2011, A&A, 535, A20
Bosch-Ramon, V., Barkov, M.V., Khangulyan, D., Perucho, M. 2012, A&A, 544, 59
Chernyakova, M., Neronov, A., Aharonian, F., Uchiyama, Y., Takahashi, T. 2009, MNRAS, 397, 2123
Dubus, G., Cerutti, B. 2013, A&A, 557, A127
Dubus, G. 2013, A&ARv, 21, 64
Eichler, D., Usov, V. 1993, ApJ, 402, 271
Hummel, W., Vrancken, M. 2000, A&A, 359, 1075
Johnston, S., Manchester, R. N., Lyne, A. G., Bailes, M., Kaspi, V. M., Qiao, G., D'Amico, N. 1992, ApJ, 387, L37
Johnston, S., Ball, L., Wang, N., Manchester, R.N. 2005, MNRAS, 358, 1069
Khangulyan, D., Aharonian, F. A., Bogovalov, S. V., Ribo, M. 2012, ApJ, 752, L17
Kong, S. W., Yu, Y.W., Huang, Y. F., Cheng, K. S. 2011, MNRAS, 416, 1067
Kong, S. W., Cheng, K. S., Huang, Y. F. 2012, ApJ, 753, 127
Lamberts, A., Dubus, G., Lesur, G., Fromang, S. 2012, A&A, 546, A60
Moldón, J., Johnston, S., Ribó M., Paredes, J. M., Deller, A. T. 2011, ApJ, 732, L10
Negueruela, I., Ribó, M., Herrero, A., Lorenzo, J., Khangulyan, D., Aharonian, F.A. 2011, ApJ, 732, L11
Neronov, A., Chernyakova, M. 2007, Ap&SS, 309, 253
Pavlov, G. G., Chang, C., Kargaltsev, O. 2011, ApJ, 730, 2
Shannona, R.M., Johnston, S., Manchester, R.N. 2014, MNRAS, 437, 3255
Stawarz, L, Petrosian, V. 2008, ApJ, 681, 1725
van Soelen, B., Meintjes, P. J., Odendaal, A, Townsend, L.J. 2012, MNRAS, 426, 3135
Wang, N., Johnston, S., Manchester, R. N. 2004, MNRAS, 351, 599
Waters, L.B.F.M., Taylor, A.R., van den Heuvel, E.P.J., Habets, G.M.H.J., Persi, P. 1988, A&A, 198, 200
Wood, K. S., Caliandro, G.A., Cheung, C.C., Li, J., Torres, D.F. (*Fermi*/LAT Collaboration) 2014, ATel, 6225, 1